JJMIE

Volume 19, Number 3, Sep. 2025
ISSN 1995-6665
Pages 500– 514
https://doi.org/10.59038/jjmie/190303
Editor-in-Chief: Prof. Ali M. Jawarneh

Jordan Journal of Mechanical and Industrial Engineering

Analysis of Discharge Behaviour and Heat Generation at in the 18650 Lithium Ion Battery Cell

Kanhaiya P. Powar*, Sharad D. Patil

Department of Mechanical Engineering, K.E. Society's Rajarambapu Institute of Technology, Rajaramnagar affiliated to Shivaji University, Kolhapur, Islampur, 415414, India.

Received 16 Feb 2025 *Accepted 28 Jul 2025*

Abstract

The rapid adoption of electric vehicles has heightened the demand for high-performance lithium-ion batteries (LiBs), where effective thermal management is critical to ensuring safety, reliability, and lifespan. This study aims to experimentally investigate the discharge behaviour and heat generation characteristics of a commercial Samsung 18650 LiB cell at varying discharge rates (DRs), and to develop a predictive model for heat generation. The cell was discharged at 1C, 2C, and 3C in constant current mode, while measuring voltage drop and surface temperature. Bernardi's model was employed to estimate the rate of heat generation (RHG). Results show that RHG increased with DR, recorded as 4.18 W, 8.05 W, and 11.37 W for 1C, 2C, and 3C, respectively. The corresponding surface temperature rises were 11.8°C, 16.8°C, and 20.2°C, with temperature non-uniformities of 1.5°C, 2.4°C, and 3.7°C. A polynomial-based mathematical model was developed using MATLAB to predict RHG with high accuracy, achieving RMSE values of 0.0315, 0.0708, and 0.1163, respectively. These findings establish a quantitative foundation for battery thermal behavior, providing essential data for the design and simulation of battery thermal management systems (BTMS). Future work may extend this modeling to different cell chemistries and integrate it with real-time BTMS strategies. Overall, this study contributes a reliable framework for thermal performance prediction in cylindrical LiB cells under dynamic discharge conditions.

Keywords: Heat generation; Lithium Ion Battery;Joule heating; Entropic heating; Curve fitting.

Abbreviations

BMS	Battery management system
BTMS	Battery thermal management system
CPCM	Composite phase change material
DoD	Depth of discharge
DR	Discharge rate
ECM	
EV	Electric vehicle
HEV	Hybrid electric vehicle
ICEV	Internal combustion engine vehicle
LiB	Lithium ion battery
OCV	Open circuit voltage
PCM	Phase change material
RHG	Rate of heat generation
RMSE	Root mean squared error
SSE	Sum of squares due to error
SoC	State of charge
SSR	Sum of squares of regression
SST	Total sum of squares
USD	United States dollar

Nomenclature

C_p	Specific heat of cell, J/kg-K
F	Faraday's constant
I	Discharge current, Amp
m	Mass of the cell, kg
Q_{gen}	Rate of heat generation, W
Δs	Entropy change
T_1	Cell surface temperature near cathode, ºC
T_2	Cell surface temperature at mid surface, ºC
T_3	Cell surface temperature near anode, ºC
T_h	Higher cell surface temperature, ºC
T_l	Lower cell surface temperature, ºC
U	Open circuit voltage, V
V	Cell potential, V

1. Introduction

For over a century, human society has been heavily dependent on vehicles driven by internal combustion engines (ICEVs) for the purpose of transportation. However, these vehicles have now become a significant contributor to air pollution, as they release various harmful gases including oxides of nitrogen (NO_x), carbon monoxide (CO), oxides of sulphur (SO_x), unburnt hydrocarbons (UHCs), carbon dioxide (CO_2), and particulate matter (PM). These circumstances have resulted in severe impact on the environment, leading to climatic changes and potential risks to human well-being. Furthermore, the depletion of fossil fuel reserves has emphasised the imperative need to transition towards the

* Corresponding author e-mail: powarkanha05526@gmail.com.

electrification of the automotive industry. Electric vehicles (EVs), which encompass hybrid electric vehicles (HEVs), present a promising solution due to their capacity for emitting zero tailpipe emissions, decreased reliance on fossil fuels, and the potential to utilise renewable energy sources. EVs have faced various obstacles, including issues related to their weight, extended charging durations, reduced lifespan, safety considerations, and limited range for extended journeys. However, continuous research and development endeavours in battery and EV technology have proven successful in effectively mitigating these constraints. As a result, EV manufacturers have been successful in offering consumers with reliable, efficient, and economically viable transportation options, resulting in a significant surge in their global acceptance in recent times. Furthermore, the cost of energy storage has been declined substantially in the last decade owing to the advancements in the battery technology. The Roland Irle's report[1] provides comprehensive data on the sales of electric vehicles (EVs) from the financial year 2012 to 2021, highlighting the growth rate and market share of EVs in the automotive industry. The data reveals a significant upward trend in EV sales, reaching a remarkable milestone of over 6.5 million units sold in 2021[1]. The annual growth rate for EV sales stands at an impressive 108%, indicating the accelerated adoption and increasing popularity of EVs among consumers[1]. Moreover, the EV's market share has grown substantially, reaching 8.3% in 2021, compared to the 2.2% market share reported in 2018[1]. These statistics demonstrate the remarkable progress made by the EV industry, particularly after the challenging year of 2020 marked by the global Covid-19 pandemic. The encouraging growth rates and expanding market share indicate a positive trajectory for the EV market, emphasizing the increasing demand and acceptance of electric vehicles as a sustainable transportation solution.

The performance of the battery pack used to power EVs influences the performance of vehicle. The battery pack selected should exhibit enhanced performance, light weight, compact and durable. The generation of heat in the battery cell during application is the major concern to the battery manufacturers as it elevates the battery temperature. The life of the battery, performance delivery and safety is largely affected by the battery temperature. Limiting the battery temperature through an appropriate battery cooling system is an indispensable part to extent overall performance of the battery unit. Researchers are continuously developing battery thermal management system (BTMS) by adopting different approaches. Researchers [2], [3], [4], [5], [6] have developed novel BTMS for LiB employing air cooling strategies like symmetrical air-cooling[2], two-directional air-flow approach[4], air cooling coupled to water evaporation[3], distributed forced convection [5]and metal and non-metal foams[6]. BTMS by adopting liquid cooling technique was studied extensively by various researchers. [7], [8], [9], [10], [11], [12], [13] studied liquid-based active BTMS using coolants like water, nano-fluid, water-ethylene glycol mixture etc. along with novel techniques/arrangements like micro-vascular composites, mini channel aluminium tubes, circuitous channel etc. In addition to this, researchers have been investigating BTMS through employing novel techniques using phase change materials (PCM), composite phase change materials (CPCM) and heat-pipe approach.

The thermal modelling, management and monitoring of modern battery systems have been significantly enhanced with the recent studies. A numerical study of mesh choice in PCM-based BTMS simulations is reported byYousefi et al.[14] and it is found that hybrid and polyhedral meshes provide a good compromise between computational accuracy and computational cost. In another study, Yousefi et al.[15] affirmed that the integration of a nanoenhanced immersion-cooling system with an optimized flow configuration allowed effective temperature management of prismatic Li-ion battery packs to various C-rates and ambient climates. In line with this,Vakilzadeh et al.[16] enhanced heat transfer in PCM systems by incorporating negative fins and local oscillators that were strategically positioned to reduce the melting time by up to 64.3%. In the same way,Vashisht et al.[17] improved the accuracy of thermal prediction by adding temperature and depth of discharge dependent resistance to electro-thermal models to achieve a prediction error of 1.95%. It is also important to monitor internal battery states; Li et al.[18] solved this problem by creating an optimised sensor topology that can reconstruct 3D electrothermal profiles in large battery packs with an error of less than 2%. To estimate SOP correctly, Chen et al.[19] proposed a patented iterative power command technique that can be used in different states of charge. Modeling-wise, Yao et al.[20] emphasized the significance of parameter tuning of P2D models on high-energy and high-power lithium-ion cells, especially at high C-rates. Madani et al.[21] reviewed major aging processes and modeling approaches in LiBs, especially focusing on the factors that have an impact on the lifetime and on the recent progress in accurate determination of residual useful life. In another study, Madani et al.[22] provided an in-depth overview of the temperature-related aging of LiB, namely, the degradation of the solid electrolyte interphase, lithium plating, and the loss of coulombic-efficiency in extreme operational conditions. Continuing the discussion of the alternative technologies, Shabeer et al.[23] explored the suitability of metal-air batteries as range extenders in EVs, and the trade-offs between energy density, performance, and cost. All these contributions point towards the need of proper modeling, effective cooling, real-time sensing, and alternative chemistries to come up with reliable and high-performance battery systems.

Evaluation of quantity of heat produced in a battery is a prerequisite step to outline BTMS. Numerous researchers have attempted to evaluate heat production in batteries by employing diverse techniques, such as the calorimeter method, heat flux measurement, and the Bernardi model, among others. Chen et al. [24] conducted experimental evaluation of heat generation from prismatic LiB at discharge rate (DR) of C/4, C/2, 1C, 2C and 3Cusing battery calorimeter. COMSOL multi-physics based analytical model was developed by Fu et al. [25] to estimate thermal distribution within lithium ion ($LiNi_{1/3}Co_{1/3}Mn_{1/3}O_2$) pouch cell at higher rates of discharge. Drake et al. [26]estimated heat generation within 26650 $LiFePO_4$ cylindrical cell through measurement of heat flux and cell surface temperature

from the cell at DR of 1C, 1.9C, 3.9C, 5.8C, 7.7C and 9.6C. Manikandan et al. [27]employed accelerating rate calorimeter to measure total heat generated in 18650 cylindrical LiB cell using NCA and NMC as cathode material and graphite as anode at charge and DR of 3C/4, C/2, 1C, 2C. Neupane et al. [28] experimentally measured the entropy coefficient, specific heat capacity and heat generation at DR of 1C to 4C from $LiFePO_4$ pouch cell. In the research study conducted by Kantharaj and Marconett[29], the RHG in LFP, NMC, and LMO cells was examined at different DRs and in different cell configurations. It was revealed that the quantity of heat generation at cathode is higher as compared to the anode. The mechanism of heat generation in the LiB as well as electrochemical reactions occurring in the LiB was discussed in detail by Raijmakers et al. [30]. Wang et al. [31] measured heat generation from 18650 cylindrical lithium ion cell during charge and discharge and validated the results with analogy and curve fitting simulation methods.Inui et al.[32] introduced a novel equivalent circuit-based method to estimate heat generation in LiBs during charge/discharge, proving its validity and necessity through successful comparisons with conventional methods and measured calorimeter data for different current patterns. Zhang et al. [33] developed a novel non-destructive method to measure heat generated within the anode and cathode of the LiB cell at 0.5C. The results showed that the heat generation at cathode is far more than the heat generation at anode. Hu et al., [34]developed a thermoelectric-based isothermal calorimeter with a Kalman filter for precise measurement of RHG from large LiBs. This novel method assists to evaluate the entropy coefficient and internal resistance of the battery with 92% reduction in the testing time. In addition to this, Yacin et al. [35] developed a novel CNN-ABC approach for precise RHG and voltage estimation in EV battery systems at different DR, outperforming other AI methods with 1.38% RMSE and 99.72% R-square in RHG estimation. Sharma and Prabhakar[36] established a lumped parameter-based thermal model to predict thermal behavior and heat generation of cylindrical LiBs with a maximum temperature of 45.9°C and average RHG of 0.19 W, 0.47 W, 0.95 W, and 1.5 W at 0.5C, 1.0C, 1.5C, and 2.0C, DR respectively, at an air temperature of 30°C. Recently, Chen et al., [37] performed a numerical analysis to investigate the effect of battery parameters and SOC on heat of polarization, ohmic heat, and reversible heat generation, and discovered that concentration of lithium ions, coefficient of reaction rate, and particle radius have a substantial effect on heat of polarization. In addition, the conductivity of the electrolyte and the separator liquid volume fraction were identified as significant factors influencing ohmic heat. In order to circumvent the shortcomings of Bernardi's empirical equations, Wu et al. [38]suggested a novel method that combines experiments and a back propagation neural network (BPNN) for estimation of RHG from battery. The outcomes show that ambient temperature and discharge current have a significant impact on RHG, with BPNN producing precise predictions with a 5% error margin.

In this research work, experimentally the voltage drop and temperature built-up in the battery cell at various DRs are measured and evaluated to estimate rate of heat generation. Furthermore, a mathematical model is developed using MATLAB curve fitting tool to predict RHG at different DR.

2. Working Principle of LiB:

A LiB is comprised of four major components viz. anode, cathode, an electrolyte and a separator as illustrated in the Figure 1. The anode and cathode are negative and positive electrodes respectively and serves the purpose of energy storage and release.An electrolyte is a material with high ionic conductivity that facilitates flow of lithium ions between the electrodes[39]. A separator prevents physical contact of anode and cathode to circumvent internal short-circuit[40]. It has nano sized pores through which lithium ions can pass. During the cell charging, the lithium ions migrates from cathode to the anode material through electrolyte. Simultaneously, the electrons flow through the external circuit in the reverse direction to maintain electro-neutrality[40]. During cell discharging, the lithium ions migrate from the anode material to the cathode through electrolyte. The electro-chemical reactions taking place in the cell during charge/discharge for lithium cobalt oxide as cathodeis illustrated in equation (1), (2) and (3) adopted from [40],

At cathode: $$LiC_OO_2 \underset{Discharge}{\overset{Charge}{\rightleftharpoons}} Li_{(1-x)}C_OO_2 + xLi^+ + xe^- \quad (1)$$

At anode: $$6C + xLi_+ + xe^- \underset{Discharge}{\overset{Charge}{\rightleftharpoons}} Li_xC_6 \quad (2)$$

Reactions: $$LiC_OO_2 + 6C \underset{Discharge}{\overset{Charge}{\rightleftharpoons}} Li_{(1-x)}C_OO_2 + Li_xC_6 \quad (3)$$

Figure 1. Working principle of LiB [39]

3. Approximation of Rate of Heat Generation

The primary step in the development of an effective BTMS requires careful quantification of heat produced during battery operation. Lai et al. [41] listed three different approaches for estimating heat generation in the battery viz. adopting Bernardi equation, experimental tests and by using electro-chemical coupling model. In addition to this, various researchers have presented theoretical approaches to predict RHGs by considering effect of different electrochemical parameters [26]. The Bernardi model given in equation (4) is a commonly employed theoretical model for heat generation estimationadopted from [42],

$$Q_{gen} = I(U-V)-IT(\partial U/\partial T) \quad (4)$$

where, I, V, U and T are the current, voltage, Open-Circuit Voltage (OCV) and temperature respectively. The first term in the equation represents heat generation caused Joule heating or cell polarization while the second term represents heat produced owing to entropic changes or entropic heat [26], [43], [44]. The entropy changes can be evaluated by the equation (5) adopted from[41],

$$\Delta S=nF(\partial U/\partial T) \quad (5)$$

In equation (2), F is the Faraday's constant which indicates the amount of electricity that is carried by 1 mol of electrons (96485 C/mol) and n represents the number of electrons contributing to the reaction (n=1 for LiB). By rearranging the terms in equation (2) for the term (∂U/∂T), the equation (1) can be modified as,

$$Q_{gen} = I(U-V)-IT(\Delta S/nF) \quad (6)$$

The quantity ΔS represented in equation (6) can be calculated by using the equation (7). Equation (7) is a standard thermodynamic relation for entropy change at constant specific heat[45][35],

$$\Delta S=mC_p ln(T_2/T_1) \quad (7)$$

The change in temperature can be obtained experimentally during charge/discharge of the cell.

In this work, an attempt is made to develop a mathematical model to predict RHG from the cell based on discharge time. Since, the heat generation behavior of the cell changes with the DR, a separate mathematical model (polynomial function) is developed to predict the behavior of the cell for each DR. The goodness (accuracy) of the fit is evaluated by measuring parameters like sum of squares due to error (SSE), R-square value, root mean squared error (RMSE) and adjusted R-square as provided in the Mathworks documentation [46].

SSE measures the total deviation of the calculated values from the fit and actual values. The SSE is expressed as, (adopted from [46])

$$SSE = \sum_{i=1}^{n} w_i(y_i - \hat{y}_i)^2 \quad (8)$$

The smaller value of SSE indicates smaller error and usefulness of the fit for prediction. The sum of squares of the regression (SSR) is given by equation (9), (adopted from [46])

$$SSR = \sum_{i=1}^{n} w_i(\hat{y}_i - \bar{y}_i)^2 \quad (9)$$

Total sum of squares (SST) can be calculated by using equation (10), (adopted from [46])

$$SST = \sum_{i=1}^{n} w_i(y_i - \bar{y}_i)^2 \quad (10)$$

The statistic R-square is the square of the correlation between the actual values and the predicted values from the fit. It is the ratio of SSR and SSTand is calculated by equation (11), (adopted from [46])

$$R - square = \frac{SSR}{SST} = 1 - \frac{SSE}{SST} \quad (11)$$

where, SST=SSR+SSE. The value of R-square should be close to 1. Similarly, the adjusted R-square value indicates the quality of the fit. It is expressed as, (adopted from [46])

$$adjusted\ R - square = 1 - \frac{SSE(n-1)}{SST\ (v)} \quad (12)$$

n indicates the number of data point and v indicates number of independent pieces of information. The value of adjusted R-square close to the 1 indicates better fit performance. RMSE statistic is given by equation (13), (adopted from [46])

$$RMSE = \sqrt{\frac{SSE}{v}} \tag{13}$$

The value of RMSE should be smaller as possible (close to 0) as it indicates higher usefulness of the model for the prediction.

4. Experimental Setup

In order to estimate the rate of heat generated in the 18650 cell, it is vital to have the temperature rise and voltage drop pattern during the discharge. A series of tests were conducted on the selected battery cell to get temperature rise and voltage drop statistics.

4.1. Experimental Apparatus:

For experimental investigation, a commercial LiB cell with 18650 configuration provided by Samsung, Korea was selected. The cell has a nominal voltage of 3.7V and 2500mAh capacity.

It comprises of lithium cobalt oxide ($LiCoO_2$) as a cathode material and graphite as anode material [47]. Technical specifications of the cell used in this study are tabulated in the Table 1.

Table 1. Technical specifications of the cell used in this study

Specification	Details
Cell Type	Cylindrical (18650)
Manufacturer	Samsung SDI
Nominal Voltage	3.7 V
Capacity	2500 mAh
Anode Material	Graphite
Cathode Material	Lithium Cobalt Oxide ($LiCoO_2$)
Electrolyte	Lithium salt in organic solvent
Cell Chemistry	Li-ion

To measure the cell temperature, three T-type thermocouple were mounted on the cell surface namely near positive tab, near negative tab and at cell mid surface. Copper-constantan thermocouple (Type-T) with fibre-glass insulation provides measurement inaccuracy of ±0.75% and gives effective measurement in the range of -200 °C to +350 °C. The measurement sensitivity of the thermocouple used is 55 µV/°C. Figure 2(a) and 2(b) depicts schematic layout and pictorial view of thermocouple arrangement over cell surface respectively. These thermocouples also helps to measure the temperature variation on the cell surface as a result of variable heat generation at cathode and anode. An electronic loading device enables discharging of battery cell at various DRs by altering the discharge current. EB tester software provided with the discharging device enables computerized control of discharge current and recording of test data. Multichannel temperature data acquisition system provided by Nimbus technologies, India (DL-35W model) with 16-channels was used to record cell surface temperature data. The opposite end of the thermocouples were linked to the data acquisition system channels.The anode and cathode terminals of the cell were connected to the discharging device to enable loading the cell.

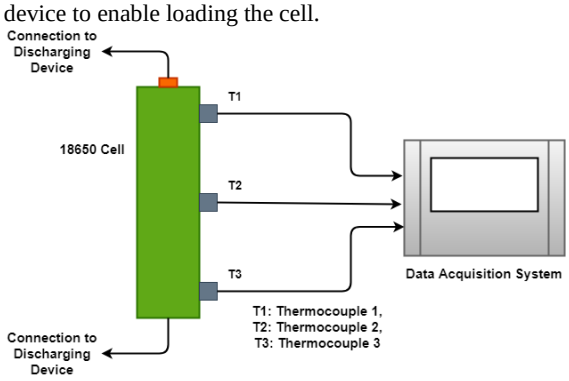

(a)

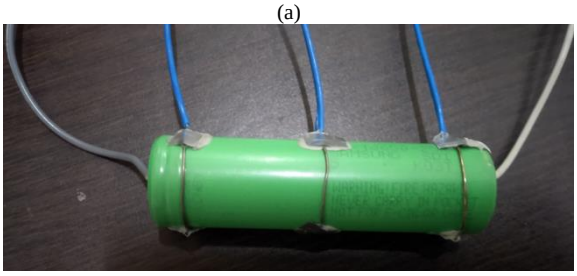

(b)

Figure 2. Thermocouple arrangement over cell surface (a) schematic layout, (b) pictorial view

Computerized control of discharging device was accredited by connecting it to the computer system employed with EB Tester software which records the cell potential during the cell discharge. Figure 3 displays the pictorial view of laboratory test setup.

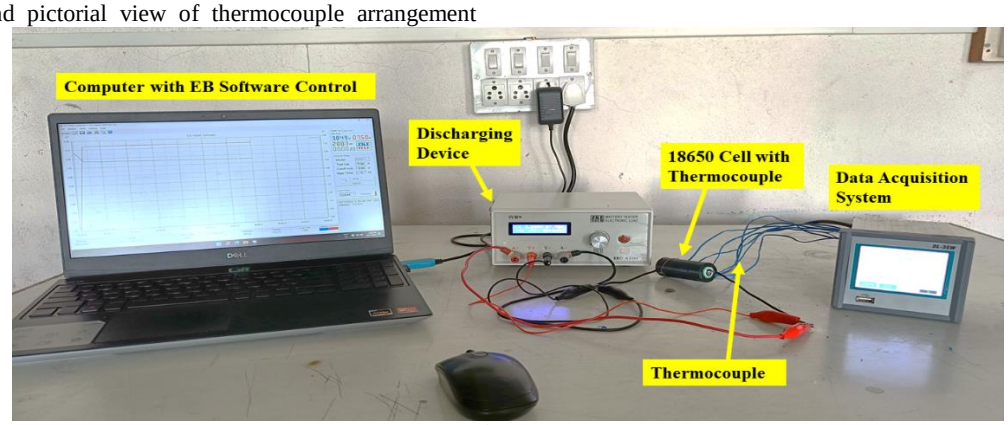

Figure 3. Laboratory test setup

To record the rise in temperature and voltage drop data of the cell, three tests were conducted at different DRs viz. 1C, 2C and 3C,where 1C represents a discharge current equal to the cell's nominal capacity (2.5 A for a 2500 mAh cell).In each test, the cell was fully charged using a TP4056 LiB charging module which operates on constant-current mode. Using the experimental test setup as shown in Figure 3, cell was discharged up to the cut-off voltage at various DR. The discharge current required to load the cell was estimated by using equation (14),adopted from [33],

$$I = R_C C \tag{14}$$

where, I represents required discharging current in A, Rc is the rated capacity of the cell in Ah and C is the DR. Table 1 specifies the discharge current and the discharge time at different DR.

Table 1. Discharge current and time for various discharge rates

Discharge Rate	Discharge Current (A)	Discharge Time (min)
1C	2.5	60
2C	5	30
3C	7.5	20

4.2. Data Processing:

The experimental measurements T_1, T_2 and T_3 refers to the cell surface temperature near positive tab, cell mid surface and near negative tab. Due to the variable heat generation at the electrode, these temperatures vary with each other as discharge proceeds. The higher and lower cell surface temperatures are defined by equation (15) and (16) respectively. While, the deviation in the cell surface temperature is defined by equation (17).

$$T_h = max(T_1, T_2, T_3) \tag{15}$$

$$T_l = min(T_1, T_2, T_3) \tag{16}$$

$$T_{diff} = T_h - T_l \tag{17}$$

For estimation of heat generation rate, the higher cell surface temperature (T_h) is regarded as cell surface temperature in subsequent analysis.

4.3. Experimental Uncertainty:

Regardless of the precautions taken during the experimental tests, uncertainties and errors may originate in an experiment. These uncertainties are caused due variety of factors such as selection of test equipment, the state of repair and calibration, the surrounding factors, methods of recording and the test design. It is critical to remember that experimental errors are unavoidable and hence, an uncertainty analysis is required to determine the validity of the experimental tests. The end result of any experiment is determined from primary measurements. The error in the end result is computed from the maximum error in any parameter used to calculate the result. In the present work, the cell potential and cell surface temperature were measured experimentally to compute the RHG, depth of discharge (DoD), temperature rise. The accuracy and percentage uncertainty in the measurement of temperature and cell potential is presented in the Table 2. The total uncertainty in the measurement is calculated by using equation (18) adopted from [48],

$$\begin{aligned} &Total\ Uncertainty\ (\%) \\ &= [(Uncertainty\ of\ T_1)^2 \\ &+ (Uncertainty\ of\ T_2)^2 \\ &+ (Uncertainty\ of\ T_3)^2 \\ &+ (Uncertainty\ of\ Voltage)^2]^{1/2} \end{aligned} \tag{18}$$

The total uncertainty of ±1.64% is well within the permissible range.

Table 2. Accuracy and percentage uncertainty in the cell potential and temperature measurement

Parameter	Accuracy	Uncertainty (%)
Cell Potential	±0.04 V	±1
Temperature	±0.3 °C	±0.75

4.4. Repeatability Test:

In order to evaluate the reproducibility and consistency of the experimental test results, a repeatability test was conducted. As a part of this test, the cell discharge test at 1C DR was repeated six times under identical test conditions with minimal sources of variation. The results of repeatability tests in the form of mean and standard deviation are presented in the Table 3. The test results confirms the precision and reliability of test procedure as the standard deviation (0.70%) is well within permission range of ±5%.

Table 3. Results of repeatability test

Parameter	Mean	Standard Deviation
T_1	37.5 °C	0.2639
T_2	35.8 °C	0.2228
T_3	33.8 °C	0.1751
V (at 1500s)	3.368V	0.0283

5. Results and Discussion:

5.1. Discharge Behavior of the Cell:

The discharge behaviour of LiB cell under test at 1C, 2C and 3C DRis depicted in the Figure 4(a). The profile of discharge curves represented are identical to the typical discharge curves for LiB. Three clearly visible zones can be observed for each discharge curve. The initial part of the curve represents non-linear correlation between the cell potential and the time. During this part, the cell potential drops rapidly from maximum charge voltage to 3.92V, 3.76V and 3.72V for 1C, 2C and 3C DR respectively. The second part represents linear correlation between cell potential and the discharge time with constant drop in cell voltage with time. During the discharge, the cell remains in the second zone for a significant period of time contributing 82-85% of the total discharge time. The third part of the curve represents non-linear correlation between the cell potential and the discharge time. In this zone, the cell potential drops at rapid rate up to the cut-off voltage. At any point during the discharge, the cell voltage is always less than the open circuit voltage due to the internal resistance of the cell and polarization of the active materials. Furthermore, as the discharge proceeds the internal resistance of the cell increases owing to the polarization effects in the cell, accumulation of products of discharge, activation polarization as well as concentration polarization. As a consequence, the cell potential

progressively drops during the discharge till cut-off voltage which in turn brings down the power delivered by the cell. Additionally, increase in the discharge current at higher DRs escalates the cell internal resistance resulting in the more tilted discharge curve profile. Subsequently, at any point during the discharge, the cell potential decreases with increase in the DRs.The figure 4(b) shows the cell voltage drop from fully charged condition to the cut off voltage with discharge capacity at allDRs under investigation. The relative capacity was recorded as 94.72% for 1C DR, 92.2% for 2C DR, and 90.8% for 3C DR, indicating a decreasing trend with higher DRs. Additionally, it was discovered that for lower DRs, the cell voltage was higher at the same discharge power. For instance, at 1C, 2C, and 3C DRs, the recorded cell voltage was 3.4V, 3.3V, and 3.2V, respectively, at a discharge power of 1000 mAh.

5.2. Temperature Rise:

The change in cell surface temperature with discharge time at various rates of discharge is shown in the Figure 5. The results of the experiment indicate that the cell surface temperature increases with rising DRs. The cell surface temperature increases from an initial value of 25.7 °C to 37.5 °C, 42.6 °C, and 46 °C for DRs of 1C, 2C, and 3C, respectively. This increase in temperature is primarily attributable to the increased cell resistance caused by greater discharge currents. The increased resistance causes a rapid drop in voltage, which increases heat production via the Joule heating phenomenon. As a result, the temperature rise is more pronounced for the 3C DR, with a temperature increase of 20.2 °C compared to 11.8 °C and 16.8 °C for the 1C and 2C DRs, respectively as depicted in the Figure 6.

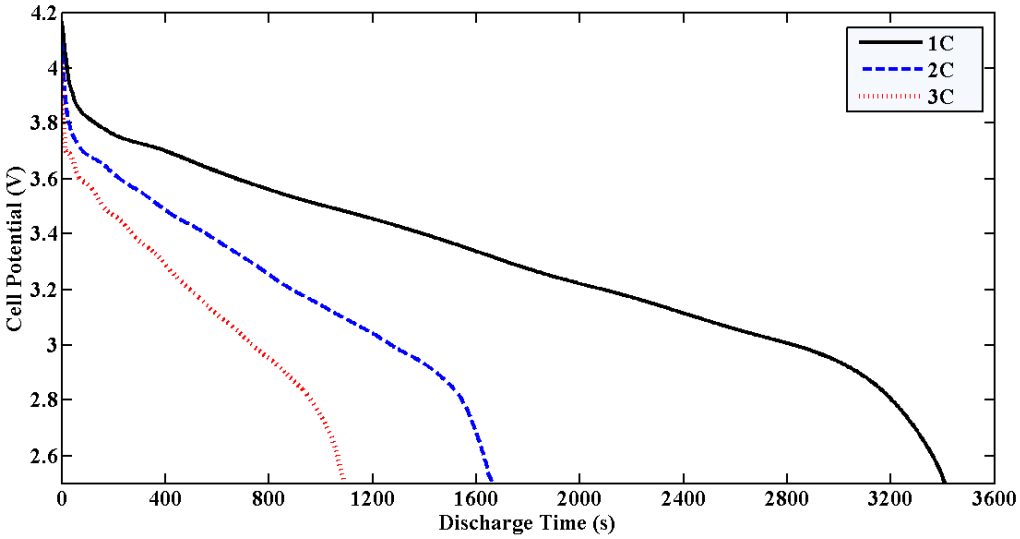

(a)

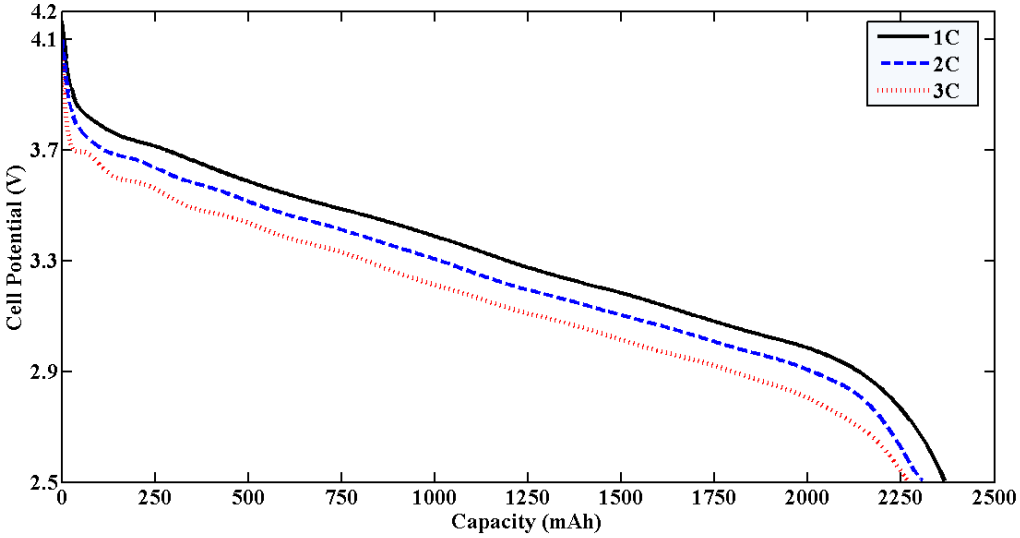

(b)

Figure 4. Discharge curves at DR of 1C, 2C and 3C with (a) discharge time, (b) discharge capacity

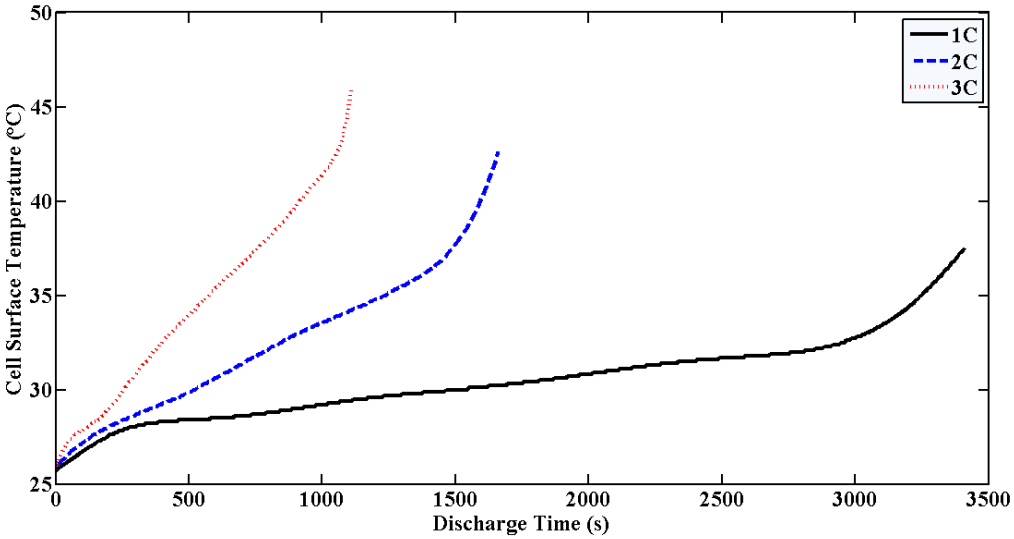

Figure 5. Cell surface temperature at DR of 1C, 2C and 3C

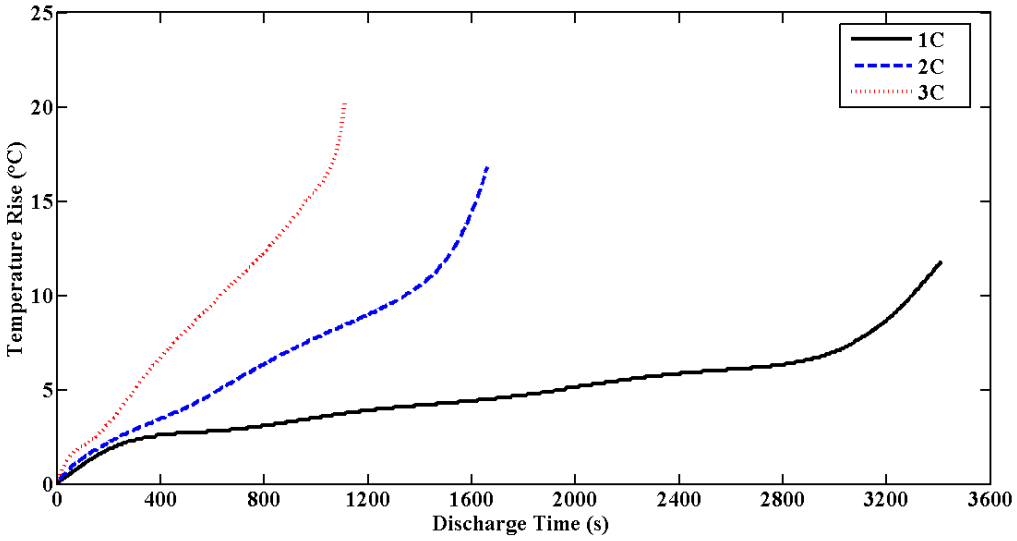

Figure 6. Rise in cell surface temperature with time at DR of 1C, 2C and 3C

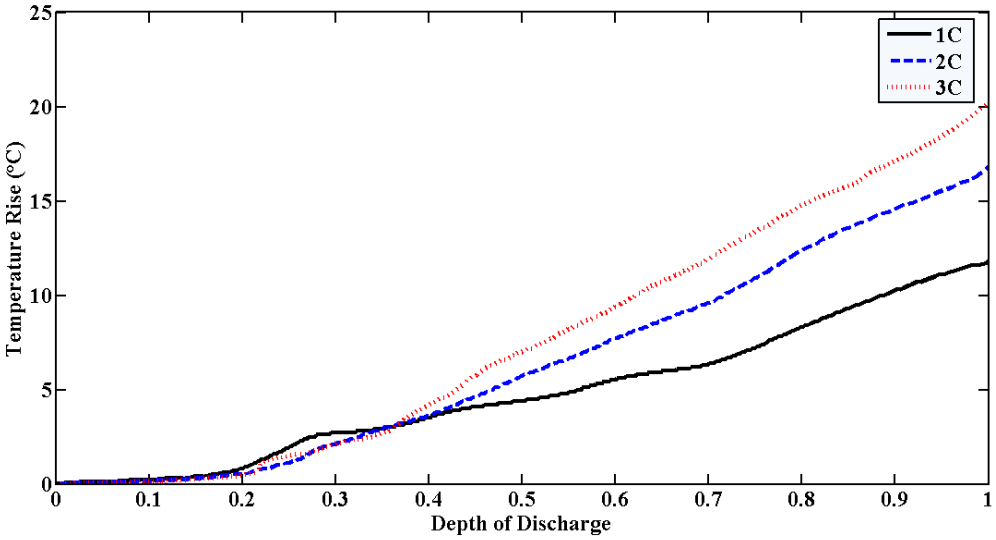

Figure 7. Rise in cell surface temperature with DoD

For sake of comparison, the cell surface temperature rise with depth of discharge is plotted in Figure 7. It confirms a higher rate of temperature rise at higher DRs as a result of accelerated cell polarization and increased cell resistance. For example, at 0.5 DoD, the temperature rise observed for 1C, 2C and 3C DR is 4.5ºC, 6.1ºC and 7.2ºC respectively.

5.3. Deviation in the Cell Surface Temperature:

Beside the temperature rise, the temperature uniformity in the battery cell is a major concern. To evaluate it, the surface temperature of the cell is measured at three locations viz. near cathode, at mid surface and near anode. Initially, uniform cell surface temperature was observed. As discharge progressed, the variations in the temperature readings was observed leading to temperature non-uniformity in the cell. This is attributed to the variable heat generation in the cell. During the cell discharge, Li ions travels from anode to the cathode due to which heat generation at the cathode is higher than that of anode. As a result of this, the temperature recorded by the T_1 thermocouple is higher than T_3. The deviation in the cell surface temperature for 1C, 2C and 3C DRis demonstrated in the Figure 8(a), 8(b) and 8(c) respectively. The temperature non-uniformityat the end of discharge was recorded 1.5 °C, 2.4 °C and 3.7 °C at 1C, 2C and 3C DR. It is clear that, higher rate of heat generation at higher DRs increases temperature non-uniformity in the cell.To ensure efficient working of the battery, the temperature non-uniformity should be less than 5 °C. According to the Arrhenius theory, the localized overheating of the cell speeds up electrochemical reactions which in turn accelerates aging of electrodes and consequently aging of the cell[47].

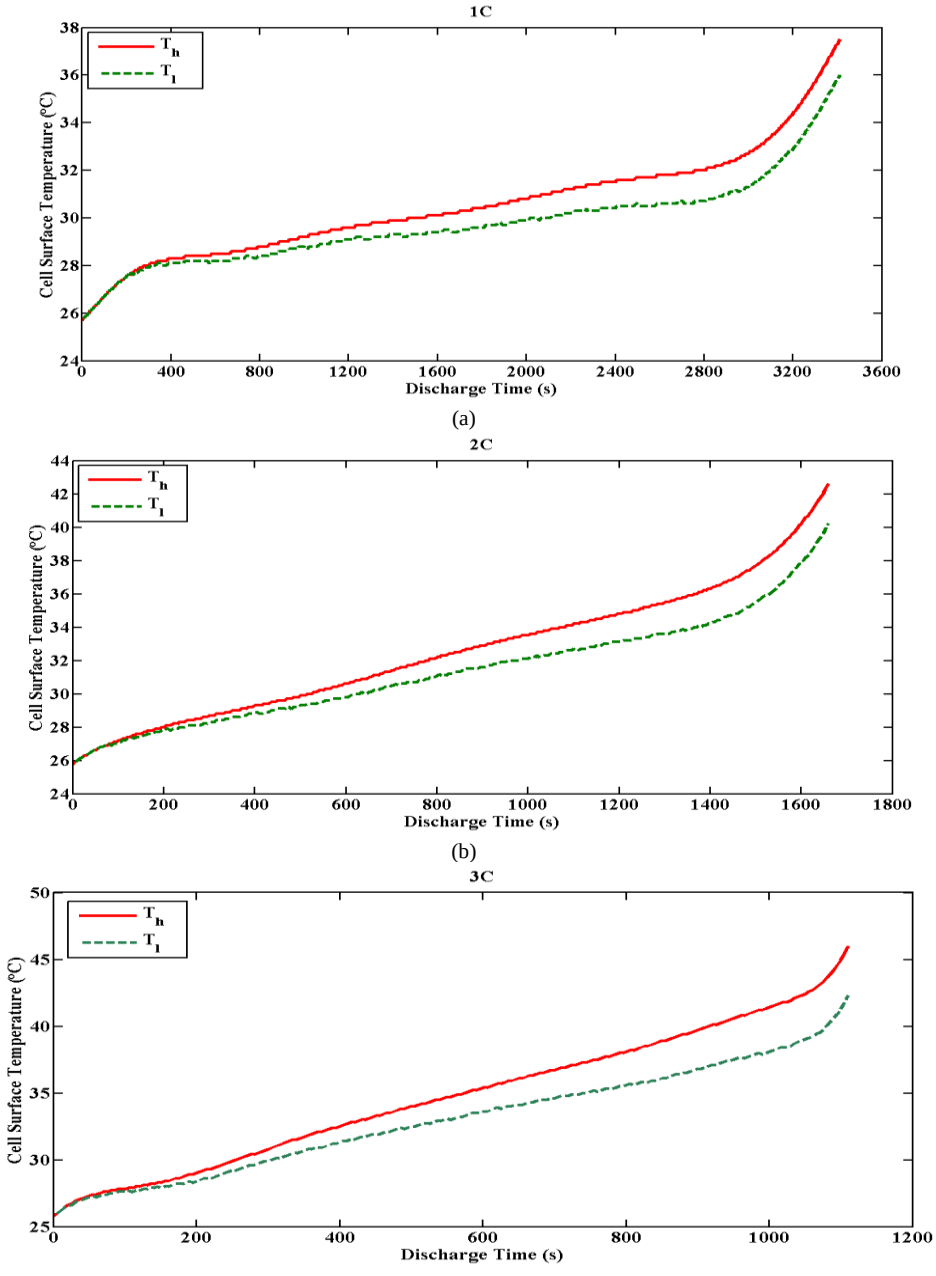

Figure 8. Deviation in the cell surface temperature at (a) 1C, (b) 2C, (c) 3CDR

5.4. Heat Generation in the Cell:

Heat generation due to Joule heating is estimated by using the first term in equation (4) using the cell potential test results. While, the entropic heat generation is estimated by calculating entropy changes during the discharge using equation (7) and temperature test data available from experimental tests. The amount of heat produced with time at various DR in the battery cell is depicted in Figure 9. When cell approaches cut-off voltage, the heat generated in the cell is 4.18W, 8.05W and 11.37W respectively for 1C, 2C and 3C DR. Increasing the discharge current causes the sudden drop in cell potential and speeds up internal chemical reactions, which causes a higher rate of heat generation at higher DRs.

5.5. Mathematical Modeling:

A MATLAB based curve fitting tool was used to develop mathematic model to compute heat generation in the SAMSUNG 18650 LiB cell at various DRs. The accuracy of the mathematical model (fit) increases with the order of polynomial function, a higher order polynomial function was used to predict heat generation on the basis of depth of discharge. The polynomial function is given in equation (19),

$$Q_{gen}(t) = p_1 + p_2(t) + p_3(t)^2 + p_4(t)^3 + p_5(t)^4 + p_6(t)^5 + p_7(t)^6 + p_8(t)^7 + p_9(t)^8 \quad (19)$$

where, (p_1, p_2, ….p_9) are the coefficients of the polynomial function. The experimentalRHG and the predicted RHG through mathematical model is plotted in the figure 10(a), 10(b) and 10(c) for various DRs.

A careful examination of the fitted curve reveals the curve fitting model predicts RHG very close to the actual values. The coefficients of 8th degree polynomial function (p1 to p9) used to predict RHG for all DRs is tabulated in the Table 3.

The mathematical model was developed based on experimental data collected under controlled conditions. The following boundary conditions were applied during the modeling process:

- Ambient temperature maintained at 25.7°C before each discharge test.
- Discharge current set at 2.5 A, 5 A, and 7.5 A corresponding to 1C, 2C, and 3C discharge rates, respectively.
- Constant current discharge up to the cut-off voltage.
- Tests were performed under natural convection in a controlled indoor environment.
- Heat loss to the surroundings was assumed to occur via convection from the cell surface, and the maximum recorded surface temperature was used for RHG calculations.
- The highest value among the three thermocouple readings (near positive tab, mid surface, and negative tab) was taken as the effective surface temperature in the model.

These boundary conditions ensured consistency across all tests and served as reliable input parameters for the development and validation of the heat generation prediction model.

Furthermore, the error in the prediction for each data point is evaluated at each DR. The error in the prediction from actual value and predicted value at each data point is depicted with the help of bar chart in Figure 11(a), 11(b) and 11(c).

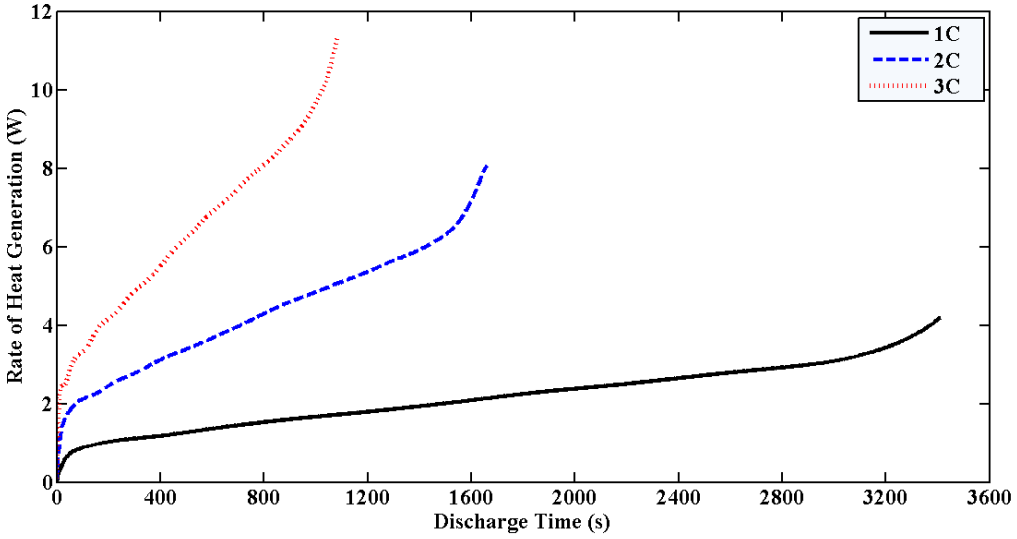

Figure 9. Heat generation in 18650 cell with respect to discharge time

Table 3. Coefficients of polynomical function

	Coefficients								
	p1	**p2**	**p3**	**p4**	**p5**	**p6**	**p7**	**p8**	**p9**
1C	$5.57*10^{-22}$	$-3.48*10^{-18}$	$1.16*10^{-14}$	$-2.20*10^{-11}$	$2.42*10^{-08}$	$-1.48*10^{-05}$	0.005259	0.397765	$5.57*10^{-22}$
2C	$1.60*10^{-19}$	$-5.00*10^{-16}$	$8.30*10^{-13}$	$-7.91*10^{-10}$	$4.36*10^{-07}$	-0.000132	0.022877	0.789738	$1.60*10^{-19}$
3C	$3.79*10^{-18}$	$-7.67*10^{-15}$	$8.30*10^{-12}$	$-5.20*10^{-09}$	$1.90*10^{-06}$	-0.000386	0.046078	1.270795	$3.79*10^{-18}$

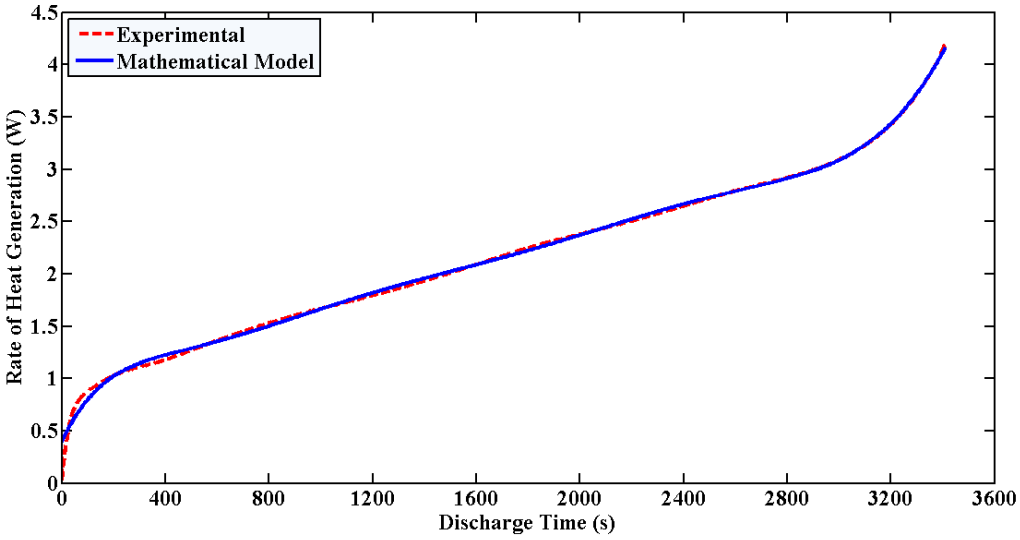

(a)

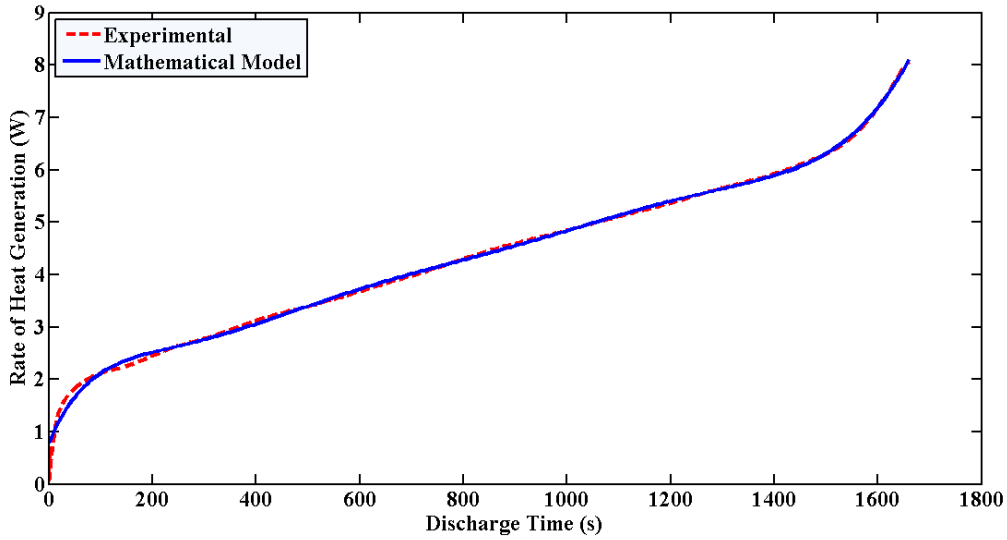

(b)

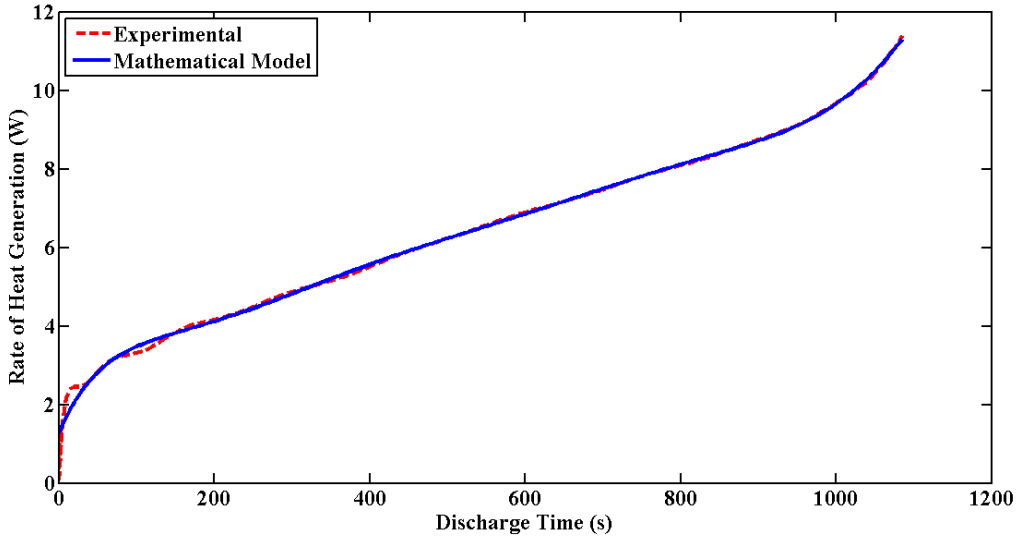

(c)

Figure 10. Comparison of heat generation rate from experimental and mathematicalmodel for (a) 1C, (b) 2C, (c) 3C

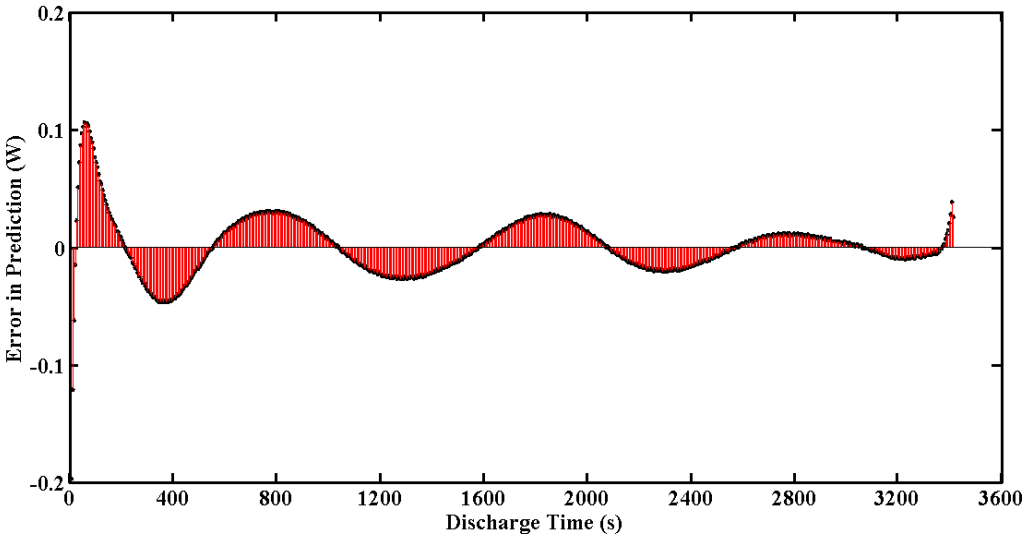

(a)

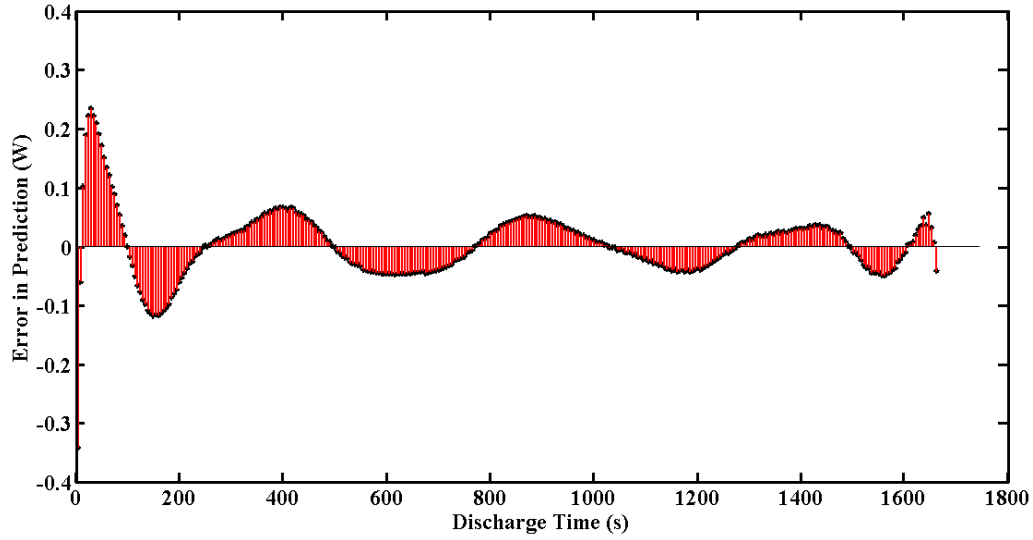

(b)

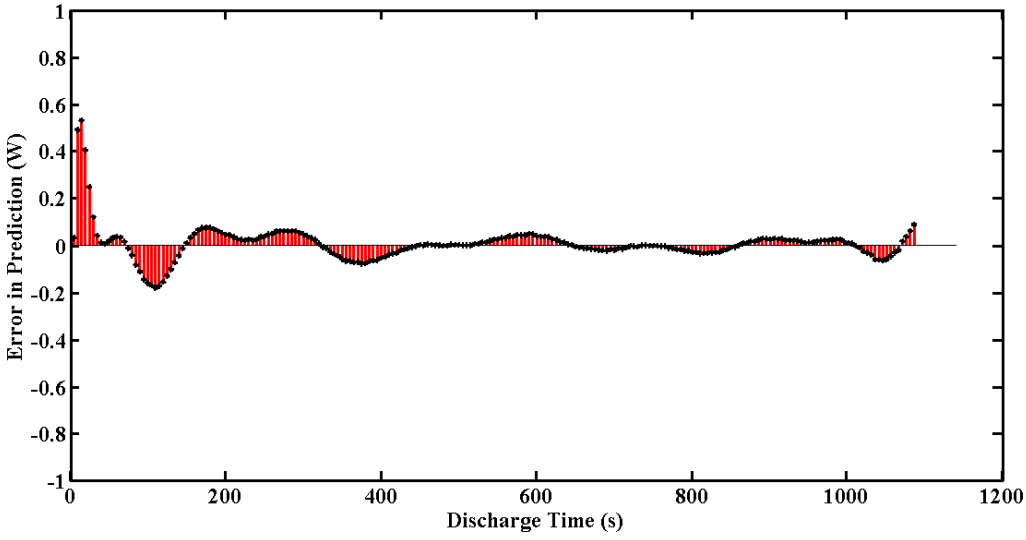

(c)

Figure 11. Error in the prediction at each data point for (a) 1C, (b) 2C, (c) 3C

It is obvious from the Figure 11 that, the errors in the prediction are very small in comparison to the quantities of heat generation at a particular data point. Additionally, the goodness of fit statistics was evaluated to check the usefulness of the fit. The values of goodness of fit statistics are tabulated in the Table 5.

Table 5: Goodness of fit statistics

	SSE	R-square	Adjusted R-square	RMSE
1C	0.6670	0.9984	0.9984	0.0315
2C	1.6237	0.9979	0.9979	0.0708
3C	2.8282	0.9975	0.9974	0.1163

All goodness of fit statistics exhibits fair degree of accuracy in the prediction. The RMSE values for 1C, 2C and 3C fit shows very minute error in the prediction.

6. Conclusion

In the present experimental research, a Samsung 18650 LiB cell was discharged at 1C, 2C and 3C rate of discharge on a constant-current discharge basis. The voltage and the surface temperature were measured to determine the rate of heat generation using Bernardi model. Moreover, a polynomial model was developed based on MATLAB to estimate RHG in terms of depth of discharge. Key findings include:

- Increased discharge rates cause a very quick voltage loss and a correspondingly shorter discharge time due to the accelerated electrochemical activity and high internal resistance.
- The high rate of voltage drop accelerated heat generation due to Joule heating phenomenon and as a result of this the RHG increases with increase in discharge current.
- In case of 3C DR, the rise in cell surface temperature and the rate of temperature rise are high in contrast to 1C and 2C rate of discharge due to higher RHG. At 3C DR the cell produces, 172.00% and 41.24% higher heat than 1C and 2C DR respectively.
- The Joule heating contributes a major share of battery heat generation as compared to the entropic heat generation.
- The mathematical model developed predicts the RHG based on battery discharge time with fair degree of accuracy at all rates of discharge.

The result provides an important grounds for design and development of BTMS for LiB.

Conflict of interest

- The authors declare that they have no conflict of interest.
- The data used in the work will be made available upon the request to author with justification.

References

[1] R. Irle, "Global EV Sales for 2021," *Global EV Sales for 2021*, Jan. 10, 2022. Available: https://ev-volumes.com/news/ev/global-ev-sales-for-2021/ [Accessed: Mar. 16, 2022]

[2] K. Chen, Y. Chen, Y. She, M. Song, S. Wang, and L. Chen, "Construction of effective symmetrical air-cooled system for battery thermal management," *Applied Thermal Engineering*, vol. 166, p. 114679, Feb. 2020, doi: 10.1016/j.applthermaleng.2019.114679

[3] G. Fang *et al.*, "Thermal management for a tube–shell Li-ion battery pack using water evaporation coupled with forced air cooling," *RSC Adv.*, vol. 9, no. 18, pp. 9951–9961, 2019, doi: 10.1039/c8ra10433f

[4] K. Yu, X. Yang, Y. Cheng, and C. Li, "Thermal analysis and two-directional air flow thermal management for lithium-ion battery pack," *Journal of Power Sources*, vol. 270, pp. 193–200, Dec. 2014, doi: 10.1016/j.jpowsour.2014.07.086

[5] G. Karimi and X. Li, "Thermal management of lithium-ion batteries for electric vehicles: Thermal management of Li-ion battery packs," *Int. J. Energy Res.*, vol. 37, no. 1, pp. 13–24, Jan. 2013, doi: 10.1002/er.1956

[6] S. K. Mohammadian and Y. Zhang, "Temperature Uniformity Improvement of an Air-Cooled High-Power Lithium-Ion Battery Using Metal and Nonmetal Foams," *Journal of Heat Transfer*, vol. 138, no. 11, Nov. 2016, doi: 10.1115/1.4033811. Available: https://asmedigitalcollection.asme.org/heattransfer/article/doi/10.1115/1.4033811/384232/Temperature-Uniformity-Improvement-of-an-AirCooled. [Accessed: Jul. 23, 2025]

[7] S. Wiriyasart, C. Hommalee, S. Sirikasemsuk, R. Prurapark, and P. Naphon, "Thermal management system with nanofluids for electric vehicle battery cooling modules," *Case Studies in Thermal Engineering*, vol. 18, p. 100583, Apr. 2020, doi: 10.1016/j.csite.2020.100583

[8] J. Liu, H. Li, W. Li, J. Shi, H. Wang, and J. Chen, "Thermal characteristics of power battery pack with liquid-based thermal management," *Applied Thermal Engineering*, vol. 164, p. 114421, Jan. 2020, doi: 10.1016/j.applthermaleng.2019.114421

[9] H. Wang, T. Tao, J. Xu, X. Mei, X. Liu, and P. Gou, "Cooling capacity of a novel modular liquid-cooled battery thermal management system for cylindrical lithium ion batteries," *Applied Thermal Engineering*, vol. 178, p. 115591, Sep. 2020, doi: 10.1016/j.applthermaleng.2020.115591

[10] S. D. V. S. S. V. Siruvuri and P. R. Budarapu, "Studies on thermal management of Lithium-ion battery pack using water as the cooling fluid," *Journal of Energy Storage*, vol. 29, p. 101377, Jun. 2020, doi: 10.1016/j.est.2020.101377

[11] S. J. Pety, P. X. L. Chia, S. M. Carrington, and S. R. White, "Active cooling of microvascular composites for battery packaging," *Smart Mater. Struct.*, vol. 26, no. 10, p. 105004, Oct. 2017, doi: 10.1088/1361-665x/aa84e7

[12] B. Xia *et al.*, "Thermal Analysis and Improvements of the Power Battery Pack with Liquid Cooling for Electric Vehicles," *Energies*, vol. 12, no. 16, p. 3045, Aug. 2019, doi: 10.3390/en12163045

[13] C. Lan, J. Xu, Y. Qiao, and Y. Ma, "Thermal management for high power lithium-ion battery by minichannel aluminum tubes," *Applied Thermal Engineering*, vol. 101, pp. 284–292, May 2016, doi: 10.1016/j.applthermaleng.2016.02.070

[14] E. Yousefi *et al.*, "Electrochemical-thermal modeling of phase change material battery thermal management systems: investigating mesh types for accurate simulations," *International Journal of Heat and Mass Transfer*, vol. 247, p. 127107, Sep. 2025, doi: 10.1016/j.ijheatmasstransfer.2025.127107

[15] E. Yousefi *et al.*, "Liquid immersion cooling with enhanced Al2O3 nanofluid for large-format prismatic battery pack: numerical and statistical investigation," *J Therm Anal Calorim*, vol. 150, no. 5, pp. 3489–3507, Mar. 2025, doi: 10.1007/s10973-024-13979-8

[16] A. H. Vakilzadeh, A. B. Sarvestani, K. Javaherdeh, R. Kamali, and S. Panchal, "To what extent does local oscillation influence the thermal performance of finned

PCM-based energy storage systems: A numerical study," *International Journal of Heat and Fluid Flow*, vol. 114, p. 109798, Aug. 2025, doi: 10.1016/j.ijheatfluidflow.2025.109798

[17] S. Vashisht, D. Rakshit, S. Panchal, M. Fowler, and R. Fraser, "Experimental estimation of heat generating parameters for battery module using inverse prediction method," *International Communications in Heat and Mass Transfer*, vol. 162, p. 108539, Mar. 2025, doi: 10.1016/j.icheatmasstransfer.2024.108539

[18] W. Li *et al.*, "A Holistic Electrothermal Profiles Online Sensing Method With Sparse Sensor System in Large-Format Battery Pack," *IEEE Trans. Ind. Electron.*, pp. 1–10, 2025, doi: 10.1109/tie.2025.3555004

[19] J. Chen, P. Kollmeyer, S. Panchal, and Y. Masoudi, "Techniques for Measuring Battery System State of Power"

[20] Q. Yao, P. Kollmeyer, J. Chen, S. Panchal, O. Gross, and A. Emadi, "Study of High-Power and High-Energy Lithium-ion Batteries: From Parameter Analysis to Physical Modeling and Experimental Validation," in *SAE Technical Paper Series*, Detroit, Michigan, United States: SAE International, Apr. 2025. doi: 10.4271/2025-01-8372. Available: https://www.sae.org/content/2025-01-8372. [Accessed: Jul. 23, 2025]

[21] S. S. Madani *et al.*, "A Comprehensive Review on Lithium-Ion Battery Lifetime Prediction and Aging Mechanism Analysis," *Batteries*, vol. 11, no. 4, p. 127, Mar. 2025, doi: 10.3390/batteries11040127

[22] S. S. Madani *et al.*, "Exploring the Aging Dynamics of Lithium-Ion Batteries for Enhanced Lifespan Understanding," *J. Phys.: Conf. Ser.*, vol. 2968, no. 1, p. 012017, Feb. 2025, doi: 10.1088/1742-6596/2968/1/012017

[23] Y. Shabeer, S. S. Madani, S. Panchal, M. Mousavi, and M. Fowler, "Different Metal–Air Batteries as Range Extenders for the Electric Vehicle Market: A Comparative Study," *Batteries*, vol. 11, no. 1, p. 35, Jan. 2025, doi: 10.3390/batteries11010035

[24] K. Chen, G. Unsworth, and X. Li, "Measurements of heat generation in prismatic Li-ion batteries," *Journal of Power Sources*, vol. 261, pp. 28–37, Sep. 2014, doi: 10.1016/j.jpowsour.2014.03.037

[25] W. Fu, J. Li, and R. You, "Heat generation breakdown of Lithium-ion Batteries," in *Proceedings of the 2017 COMSOL Conference in Beijing*, Beijing, 2017.

[26] S. J. Drake *et al.*, "Heat generation rate measurement in a Li-ion cell at large C-rates through temperature and heat flux measurements," *Journal of Power Sources*, vol. 285, pp. 266–273, Jul. 2015, doi: 10.1016/j.jpowsour.2015.03.008

[27] B. Manikandan, C. Yap, and P. Balaya, "Towards Understanding Heat Generation Characteristics of Li-Ion Batteries by Calorimetry, Impedance, and Potentiometry Studies," *J. Electrochem. Soc.*, vol. 164, no. 12, pp. A2794–A2800, 2017, doi: 10.1149/2.1811712jes

[28] S. Neupane, M. Alipanah, D. Barnes, and X. Li, "Heat Generation Characteristics of LiFePO4 Pouch Cells with Passive Thermal Management," *Energies*, vol. 11, no. 5, p. 1243, May 2018, doi: 10.3390/en11051243

[29] R. Kantharaj and A. M. Marconnet, "Heat Generation and Thermal Transport in Lithium-Ion Batteries: A Scale-Bridging Perspective," *Nanoscale and Microscale Thermophysical Engineering*, vol. 23, no. 2, pp. 128–156, Apr. 2019, doi: 10.1080/15567265.2019.1572679

[30] L. H. J. Raijmakers, D. L. Danilov, R.-A. Eichel, and P. H. L. Notten, "A review on various temperature-indication methods for Li-ion batteries," *Applied Energy*, vol. 240, pp. 918–945, Apr. 2019, doi: 10.1016/j.apenergy.2019.02.078

[31] Z. Wang *et al.*, "Calculation methods of heat produced by a lithium-ion battery under charging-discharging condition," *Fire and Materials*, vol. 43, no. 2, pp. 219–226, Mar. 2019, doi: 10.1002/fam.2690

[32] Y. Inui, S. Hirayama, and T. Tanaka, "Detailed estimation method of heat generation during charge/discharge in lithium-ion battery using equivalent circuit," *Elect Comm in Japan*, vol. 102, no. 12, pp. 3–14, Dec. 2019, doi: 10.1002/ecj.12221

[33] J. Zhang, X.-G. Yang, F. Sun, Z. Wang, and C.-Y. Wang, "An online heat generation estimation method for lithium-ion batteries using dual-temperature measurements," *Applied Energy*, vol. 272, p. 115262, Aug. 2020, doi: 10.1016/j.apenergy.2020.115262

[34] Y. Hu, S.-Y. Choe, and T. R. Garrick, "Measurement of heat generation rate and heat sources of pouch type Li-ion cells," *Applied Thermal Engineering*, vol. 189, p. 116709, May 2021, doi: 10.1016/j.applthermaleng.2021.116709

[35] S. Yalçın, S. Panchal, and M. S. Herdem, "A CNN-ABC model for estimation and optimization of heat generation rate and voltage distributions of lithium-ion batteries for electric vehicles," *International Journal of Heat and Mass Transfer*, vol. 199, p. 123486, Dec. 2022, doi: 10.1016/j.ijheatmasstransfer.2022.123486

[36] D. K. Sharma and A. Prabhakar, "Estimation of Heat Generation and Thermal Behavior of Cylindrical Lithium-Ion Battery Under Natural Convection," in *Advances in Clean Energy and Sustainability*, Singapore: Springer Singapore, 2022, pp. 119–129. doi: https://doi.org/10.1007/978-981-99-2279-6_11

[37] Z. Chen, Y. Qin, Z. Dong, J. Zheng, and Y. Liu, "Numerical study on the heat generation and thermal control of lithium-ion battery," *Applied Thermal Engineering*, vol. 221, p. 119852, Feb. 2023, doi: 10.1016/j.applthermaleng.2022.119852

[38] C. Wu *et al.*, "Experimental and numerical studies on lithium-ion battery heat generation behaviors," *Energy Reports*, vol. 9, pp. 5064–5074, Dec. 2023, doi: 10.1016/j.egyr.2023.04.021

[39] LG Energy Solution, "Lithium-ion Battery's Structure and How It Works," *Lithium-ion Battery's Structure and How It Works*, Jul. 2022. Available: https://inside.lgensol.com/en/2022/07/lithium-ion-batterys-structure-and-how-it-works/#. [Accessed: May 03, 2023]

[40] Y. Chen *et al.*, "A review of lithium-ion battery safety concerns: The issues, strategies, and testing standards," *Journal of Energy Chemistry*, vol. 59, pp. 83–99, Aug. 2021, doi: 10.1016/j.jechem.2020.10.017

[41] Y. Lai *et al.*, "Insight into heat generation of lithium ion batteries based on the electrochemical-thermal model at high discharge rates," *International Journal of Hydrogen Energy*, vol. 40, no. 38, pp. 13039–13049, Oct. 2015, doi: 10.1016/j.ijhydene.2015.07.079

[42] D. Bernardi, E. Pawlikowski, and J. Newman, "A General Energy Balance for Battery Systems," *J. Electrochem. Soc.*, vol. 132, no. 1, pp. 5–12, Jan. 1985, doi: 10.1149/1.2113792

[43] D. Galatro, M. Al-Zareer, C. Da Silva, D. A. Romero, and C. H. Amon, "Thermal Behavior of Lithium-Ion Batteries: Aging, Heat Generation, Thermal Management and Failure," *Frontiers in Heat and Mass Transfer*, vol. 14, May 2020, doi: 10.5098/hmt.14.17. Available: https://www.techscience.com/fhmt/ v14n1/52937. [Accessed: Jul. 26, 2025]

[44] N. H. F. Ismail, S. F. Toha, N. A. M. Azubir, N. H. Md Ishak, M. K. Hassan, and B. S. Ksm Ibrahim, "Simplified Heat Generation Model for Lithium ion battery used in Electric Vehicle," *IOP Conf. Ser.: Mater. Sci. Eng.*, vol. 53, p. 012014, Dec. 2013, doi: 10.1088/1757-899x/53/1/012014

[45] M. J. Moran, H. N. Shapiro, D. D. Boettner, and M. B. Bailey, *Fundamentals of Engineering Thermodynamics*, 7th ed. Hoboken, NJ: John Wiley & Sons, 2010.

[46] D. MATLAB, “Evaluating Goodness of Fit - MATLAB & Simulink,” *Mathworks.com*. Available: https://in.mathworks.com/help/curvefit/evaluating-goodness-of-fit.html. [Accessed: May 03, 2023]

[47] Samsung SDI, “Safety Data Sheet – Model INR18650-25R,” Samsung SDI Co., Ltd., Gyeonggi-do, Korea, Jan. 2016. Available: https://files.batteryjunction.com/frontend/files/samsung/msds/SAMSUNGINR18650-25R-MSDS.pdf. [Accessed: Mar. 15, 2022]

[48] J. P. Holman, *Experimental Methods for Engineers*, 8th ed. Mc-Graw Hill Education, 2012.